

Rasmussen, K.L., et al., 2023, The source of tungsten-associated magmas in the northern Canadian Cordillera and implications for the basement: *Geology*, <https://doi.org/10.1130/G51042.1>

Supplemental Material

Methods

Figure S1

Table S1

Supplemental Dataset 1

Supplemental Dataset 2

APPENDIX 1. METHODS

U–Pb Analytical Methods

Zircons were obtained by conventional heavy liquid extraction for 18 samples taken from 10 plutons (Dataset S1) along the length of the TPS. At least 200–300 grains were hand-picked wherever sample sizes allowed, with a preference for grains with obvious cores (many samples did not contain that many grains, in which case all grains that could be physically picked up were selected), and mounted in an epoxy disc and polished to 1 μm . Imaging was done using a JEOL JSM-71000F FEG SEM operating at 15 kV and equipped with a Deben Centaurus cathodoluminescence (CL) detector at the Earth Resources Research and Analysis (TERRA) Facility in the Department of Earth Sciences, Memorial University, St. John's. CL images of >3300 zircons were used to identify potential inherited cores based on obvious resorption surfaces between zircon sectors of varying character (ie, older cores were often highly fractured, altered, and the vast majority are depleted in uranium relative to the magmatic rims). However, a visual distinction between magmatic vs inherited zircon was not always straightforward, and some bias in the resulting analyses may have been introduced by under-analyzing inherited cores that did not have these characteristics, or that were too small or altered to analyze. Internal textures identified in the CL images were also used to choose U–Pb ablation spots in grain cores of varying sizes to provide a representative dataset. Between 4 and 42% of the grains appear to contain older inherited cores, depending on the sample and the level of polish attained. Cores suspected of being xenocrystic (ie, lacking a well-developed magmatic rim) were not analyzed, or were rejected after analysis based on one or more of the following textural criteria: a) a very thin magmatic rim relative to the size of the core; b) a retained well-rounded morphology with minimal evidence for resorption; and/or c) a lack of alteration resulting in nearly ubiquitous concordance that was not typical of most of the inherited cores. These three features usually occurred together, suggesting that these zircon cores were not present in the magma long enough to have been altered or significantly resorbed and are, therefore, most likely xenocrystic in origin. If there were any doubts about this distinction, the analysis was removed from the dataset. However, it is

impossible to be certain that all analyses under consideration herein were on cores that were inherited in the melt source. Notably, cores younger than ~1400 Ma that passed our three filters may still be suspect as they represent a small but important age population. They are discussed further in “Statistical Treatment of the Data”, below, and SEM-CL images for these 6 analyses are provided in Dataset S1.

U–Pb isotope measurements were made in the Arctic Resources Laboratory at the University of Alberta using a Resolution Excimer 193 nm laser ablation system operating with an energy fluence ranging from 3.5–3.8 J/cm² measured at the ablation site and operating at 6–8 Hz (specific analysis parameters are provided in Dataset S1). The isotope measurements were performed on a Thermo Element-XR 2 mass spectrometer using a single secondary electron multiplier detector in peak hopping mode. Data collection consisted of multiple groups of 12 unknowns bracketed by at least two each of Plesovice, LH94-15 and 91500 ± FC-1 to monitor precision. Data were processed in Iolite v3.32 and optimized for ²⁰⁷Pb/²⁰⁶Pb ages using LH94-15 as the primary reference material. Zircons 91500 ± FC-1 were treated as unknowns. Reference materials data are summarized in Dataset S1.

Approximately 25% (n = 248) of the attempted inherited core analyses produced acceptable results from which segments ranging from seven to 44 seconds were trimmed to include a stable ²⁰⁷Pb/²⁰⁶Pb signal, combined with elevated ²⁰⁶Pb/²³⁸U and ²⁰⁷Pb/²³⁵U ages, measurable U²³⁸, and Pb²⁰⁴ at or near background levels. All acceptable inherited core analyses are reported in Dataset S1. Discordance (%) was calculated as: $100 * (\text{²⁰⁷Pb/²⁰⁶Pb age} - \text{²⁰⁶Pb/²³⁸U age}) / (\text{²⁰⁷Pb/²⁰⁶Pb age})$. Analyses were considered to be “concordant” if discordance was between -5% to 10%.

“Best Age” Determination

Due to the high proportion of discordant analyses in our dataset, an R modeling procedure similar to that described by Reimink et al. (2016) and demonstrated by Pryer (2017) was applied to a subset of the

acceptable inherited core analyses ($n = 170$). This procedure allows us to assess the relative likelihood of each potential lower intercept age for all data and determine if there is a dominant shared lower intercept age representing a common discordance event that fits our dataset. The code was run with a node spacing of 3 Myr and produced 249,000 chords or possible concordia lines. In this analysis, the total probability aggregated by all chords containing a single lower intercept age was summed. For instance, all the probability that was assigned by the U-Pb data to all discordia chords with a 100 Ma lower intercept age was added together. The 100 Ma–101 Ma chord probability was added to the 100 Ma–102 Ma chord which was added to the 100 Ma–103 Ma chord, etc. This produced a sum lower intercept likelihood value across a range of possible lower intercept ages. The highest likelihood lower intercept age produced by the model was ca. 105 Ma, with a secondary peak ca. 190 Ma (Fig. S1).

A maximum likelihood lower age intercept ca. 105 Ma is consistent with evidence for a widespread thermal event in the region indicated by magmatic core to magmatic rim ages determined for the TPS plutons that range predominantly from 96–112 Ma (peaking at ~103–105 Ma; Rasmussen, unpublished data) combined with autocrystic/antecrystic (i.e., magmatic) zircon ranging from 100–103 for several TPS plutons (and ranging up to 107 Ma for other plutonic suites in the area; Rasmussen, 2013), as well as widespread 106–100 Ma batholithic magmatism immediately southeast of the region (Hart et al, 2004). This dominant shared lower intercept age, therefore, likely reflects discordance caused by either partial-melting-induced Pb-loss peaking ca. 105 Ma, or inadvertently mixed analyses intersecting both inherited core and magmatic sectors (Pryer, 2017). Either way, the result is geologically reasonable and it justifies anchoring the lower intercept age at 105 Ma when calculating the upper intercept age, which is interpreted to be the true age of the inherited core with the effects of discordance effectively removed.

There is no known geological significance for the older lower intercept at ~190 Ma. However, this peak is broader and ill-defined in the likelihood spectra, so it was not used as it may be an artifact due to

discordia lines that cross clusters of points close together that are grouped purely due to statistical change (e.g., Reimink et al, 2016).

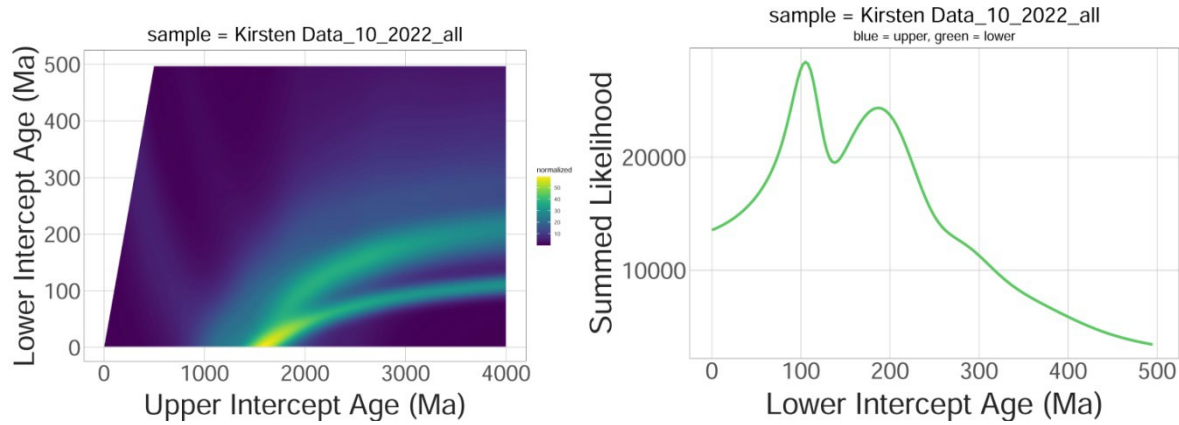


Figure S1. R outputs demonstrating the most likely lower age intercepts.

The “Best Age” determinations in Dataset S1 include concordia ages for 35 concordant analyses with an MSDW of concordance < 2.5 . For any concordant analysis with MSDW > 2.5 , as well as for all of the discordant analyses ($> 10\%$ discordance) the lower intercept was anchored at 105 Ma and the upper intercept age was calculated in Isoplot 4.15 (Ludwig, 2012). Possible error induced by inaccuracy in the lower intercept age was not included in the final 2-sigma uncertainties reported for each “best age” as Pryer (2017) demonstrated this effect to be minimal on the final dataset. The resulting upper intercept ages were used as the “Best Age” in Dataset S1 if (a) the 2-sigma error on the re-calculated upper intercept age was $< 10\%$ of the age; and (b) the re-calculated upper intercept age was within 50 m.y. (including uncertainty) of the original $^{207}\text{Pb}/^{206}\text{Pb}$ age, which was the case for the majority of analyses with $< 40\%$ discordance. Analyses not meeting these two criteria were removed from consideration for the statistical analysis, and the remaining 190 “Best Age” determinations in Dataset S1 are considered to represent the distribution of dates for the detrital zircons incorporated in the TPS magmas as inherited zircon during anatexis of the protolith rock(s).

Detrital Zircon Grouping

Due to small sample sizes for most of the available detrital zircon datasets ($n < 300$), to increase the validity of the statistical analysis units of similar provenance and age were grouped prior to comparing them with the data for inherited cores from the TPS. While this can hide intersample variations that may be significant for provenance studies (e.g., Lane and Gehrels, 2014), we are interested in the overall detrital zircon signature for a group of rocks as it is unlikely that one particular unit within a larger group would be the sole source of melt during anatexis. Thus, the TPS inherited zircon data likely comprise an assemblage of grains from multiple units within the same stratigraphic package or ‘grouping,’ and comparisons of stratigraphic groupings to the TPS dataset will ideally identify which groupings are the most likely source(s) of these inherited cores.

Groups were made comprising samples of the Muskwa assemblage ($n=88$), Wernecke Supergroup ($n = 303$), Pinguicula Group ($n = 350$), Unit Ps ($n = 202$), and the Mackenzie Mountains Supergroup ($n = 763$) due to the generally shared provenance interpretations for all samples within each of these groups, despite some intersample variation.

Published data for the Windermere Supergroup demonstrates it has two different detrital zircon signatures depending on the age of the rocks. Cryogenian samples consistently have a “Grenvillian” detrital zircon signature, which has been attributed to derivation by reworking of the older underlying Mackenzie Mountains Supergroup (Lane and Gehrels, 2014). These Cryogenian samples were placed into one group for the statistical analysis ($n = 631$). Ediacaran samples (tentatively assigned to the Windermere Supergroup in the northern Cordillera) consistently have a “cratonic” detrital zircon signature that could be attributed to either derivation by reworking of older underlying Pinguicula Group, Wernecke Supergroup, and/or possibly Muskwa Assemblage rocks. Alternatively, the “cratonic” signature observed in Ediacaran units may be a result of direct derivation from northern Laurentia, depending on the paleogeographic position of the sample. Similarly, lower Cambrian (Terreneuvian) samples display a

“cratonic” detrital zircon signature that has typically been interpreted to reflect both local recycling of older rocks and/or direct derivation from northern Laurentia (Leslie, 2009; Hadlari et al, 2012; Lane and Gehrels, 2014; Pigage et al, 2015; McMechan et al, 2017). Due to their similar “cratonic” detrital zircon signatures, the Ediacaran and lower Cambrian samples were grouped together for the statistical analysis (n=558).

Middle to late Cambrian samples (Miaolingian to Furongian) across the Selwyn Basin display “cratonic”, “Grenvillian”, and mixed detrital zircon signatures (Hadlari et al, 2012; Lane and Gehrels, 2014). This complexity is likely due to paleogeography and it probably resulted from local recycling of older units, which varied depending their position in the Selwyn Basin and local sedimentation patterns (Lane and Gehrels, 2014; Pigage et al, 2015; McMechan et al, 2017). Middle to late Cambrian samples were sub-divided into either “cratonic” (n = 343), “mixed” (n = 499), or “Grenvillian” (n = 635) groupings.

Like the middle to late Cambrian, Ordovician samples were also sub-divided into “cratonic” (n = 582) and “Grenvillian” (n = 40) groups depending on their detrital zircon signature, which also likely reflects local variation in recycled detritus.

Statistical Treatment of the Data

The Cross-correlation coefficient (R^2) for Probability Density Plots (PDPs) and Kernel Density Estimates (KDEs) were selected as the best statistical tools to determine the probability that two or more samples were derived from the same parent population of zircon. The PDP Cross-correlation metric fulfills all the criteria suggested by Saylor and Sundell (2016) for a quantitative metric of sample similarity, and is responsive to the presence, absence, magnitude and/or shape of age peaks in a cross-plot of PDPs for 2 samples. However, it cannot account for differences in age uncertainty calculations or instrument sensitivity for data generated in different labs; therefore, the KDE Cross-correlation analysis was also

employed, which uses a fixed bandwidth to remove the effect of inter-lab variation (Vermeesch, 2013). A R^2 of 1.0 is a perfect match between two samples, but values greater than >0.7 (PDP) and >0.5 (if $n > 375$; KDE) are generally indicative of derivation from the same source (see Fig. 12 in Saylor and Sundell, 2016). Both statistical tests were run to compare the sedimentary groupings against the TPS dataset with and without the 6 dates that were younger than 1400 Ma, and it was found that the influence of 6 ~ 1.0 Ga grains on the final results was minimal (i.e., R^2 varied by no more than 0.01; Dataset S2).

Unfortunately, samples with <375 analyses will negate the ability of the KDE metric to definitively identify two or more samples derived from the same parent population. The statistical analysis was mainly limited by the sample size for the TPS ($n = 190$). Randomly generated sub-samples ($n = 170$) for the TPS and the larger datasets were run 100 and 1000 times to determine if the mean R^2 remained consistent for both the PDP and KDE metrics. This study used DZstats to perform the Cross-correlation analysis using the “Intersample Compare” and the “SubSample Compare” functions (Saylor and Sundell, 2016). Results are summarized in Table S1 and in Dataset S2.

The PDP results show that the mean coefficient decreased marginally for the sub-sample tests and had a very small standard deviations, whereas the KDE results show that R^2 decreased more significantly and displays large standard deviations indicative of a greater variability during the sub-sample testing (Table S1). The consistency of the PDP sub-sample results and the preservation of cross-correlation coefficients that are >0.7 (Saylor and Sundell, 2016) or >0.75 (Gibson et al, 2021) for the sub-sampling tests are indicative of the same parent and allow interpretations to be made from the PDP statistical treatment, whereas while the KDE data are consistent with the PDP results, interpretations cannot be made due to a sample size for the TPS and many of the detrital zircon groupings of <375 . Thus, the interpretation of which detrital zircon datasets are most similar to the TPS in the text relies primarily upon the PDP results of the statistical analysis.

TABLE S1. SUMMARIZED CROSS-CORRELATION COEFFICIENTS (R^2) BETWEEN THE TUNGSTEN PLUTONIC SUITE AND THE COMPILED DATASETS

Compiled datasets	n	PDP R^2	R^2 Mean of sub-samples (n=170)						KDE R^2	R^2 Mean of sub-samples (n=170)					
			t = 100	st dev	diff. (%)	t = 1000	st dev	diff. (%)		t = 100	st dev	diff. (%)	t = 1000	st dev	diff. (%)
Muskwa assemblage (Ma)	92	0.78	N.D.*	N.D.	N.D.	N.D.	N.D.	N.D.	0.77	N.D.	N.D.	N.D.	N.D.	N.D.	N.D.
Wernecke SG (WSG)	303	0.83	0.80	0.04	5	0.80	0.04	5	0.84	0.72	0.13	18	0.71	0.14	20
Pinguicula Gp (PG)	350	0.64	0.62	0.04	6	0.62	0.04	7	0.65	0.59	0.13	22	0.58	0.15	27
unit Ps (PS)	202	0.74	0.73	0.02	3	0.73	0.02	3	0.72	0.68	0.16	24	0.66	0.17	26
Mackenzie Mountains SG (MSG)	763	0.01	0.01	0.01	70	0.02	0.01	74	0.02	0.02	0.03	123	0.02	0.03	134
Cryogenian (Cry)	631	0.03	0.03	0.02	64	0.03	0.02	55	0.02	0.04	0.04	100	0.03	0.04	119
Ediacaran to lower Cambrian (E-LC)	558	0.79	0.77	0.04	5	0.77	0.04	5	0.76	0.65	0.16	25	0.62	0.17	27
Mid- to late Cambrian, cratonic (M-LC _C)	343	0.86	0.83	0.03	4	0.84	0.03	4	0.85	0.70	0.13	18	0.70	0.14	20
Mid- to late Cambrian, mixed (M-LC _M)	635	0.23	0.22	0.06	27	0.22	0.06	26	0.23	0.23	0.10	44	0.22	0.11	50
Mid- to late Cambrian, Grenvillian (M-LC _G)	499	0.00	0.00	0.00	141	0.00	0.00	145	0.00	0.01	0.01	175	0.01	0.02	197
Ordovician, cratonic (O _C)	582	0.74	0.73	0.03	4	0.73	0.03	5	0.63	0.50	0.15	31	0.50	0.15	31
Ordovician, Grenvillian (O _G)	40	0.00	N.D.*	N.D.	N.D.	N.D.	N.D.	N.D.	0.00	N.D.*	N.D.	N.D.	N.D.	N.D.	N.D.

Note: Cell shading is gradational based on R^2 values, and bolded entries ($R^2 > 0.75$) indicate a correlation between the TPS and the compiled dataset that is indicative of derivation from the same parent source.

*N.D. = not determined.

References

- Gibson, T.M., Faehnrich, K., Busch, J.F., McClelland, W.C., Schmitz, M.D., and 237 Strauss, J.V., 2021, A detrital zircon test of large-scale terrane displacement along the Arctic 238 margin of North America: *Geology*, v. 49, p. 545–550, <https://doi.org/10.1130/G48336.1>.
- Hart, C.J.R., Mair, J.L., Goldfarb, R.J., and Groves, D.I., 2004, Source and redox controls on 256 metallogenic variations in intrusion-related ore systems, Tombstone-Tungsten Belt, Yukon 257 Territory, Canada: *Transactions of the Royal Society of Edinburgh: Earth Sciences*, v. 95, 258 p. 339–356, <https://doi.org/10.1017/S0263593300001115>.
- Hadlari, T., Swindles, G.T., Galloway, J.M., Bell, K.M., Sulphur, K.C., Heaman, L.M., Beranek, 252 L.P., and Fallas, K.M., 2015, 1.8 billion years of detrital zircon recycling calibrates a 253 refractory part of Earth's sedimentary cycle: *PLoS One*, v. 10, 254 <https://doi.org/10.1371/journal.pone.0144727>.
- Lane, L.S., and Gehrels, G.E., 2014, Detrital zircon lineages of late Neoproterozoic and 270 Cambrian strata, NW Laurentia: *Geological Society of America Bulletin*, v. 126, p. 398–271 414, <https://doi.org/10.1130/B30848.1>.
- Leslie, C.D., 2009, Detrital zircon geochronology and rift-related magmatism: central Mackenzie Mountains, Northwest Territories [M.Sc. Thesis]: Vancouver, University of British Columbia, 224 p, <https://doi.org/10.14288/1.0052744>.
- Ludwig, K.R., 2012, User's manual for Isoplot version 3.75–4.15: A 273 geochronological toolkit for Microsoft Excel: Berkeley Geochronological Center Special 274 Publication 5, 75 p.
- McMechan, M., Currie, L., Ferri, F., Mathews, W., and O'Sullivan, P., 2017, Cambrian detrital 276 zircon signatures of the northern Cordilleran passive margin, Liard area, Canada: Evidence 277 of sediment recycling, non-Laurentian ultimate sources, and basement denudation: *Canadian 278 Journal of Earth Sciences*, v. 54, p. 609–621, <https://doi.org/10.1139/cjes-2016-0127>.
- Reimink, J.R., Davies, J.H.F.L., Waldron, J.W.F., and Rojas, X., 2016, Dealing with 312 discordance: A novel approach for analysing U-Pb detrital zircon datasets: *Journal of the 313 Geological Society*, v. 173, p. 577–585, <https://doi.org/10.1144/jgs2015-114>.
- Pigage, L.C., Roots, C.F., and Abbott, J.G., 2015, Regional bedrock geology for Coal River map area (NTS 95D), southeast Yukon: *Yukon Geological Survey Bulletin* 17, 155 p.
- Pryer, L., 2017, Genesis and controls on the mineralization of the Keglovic 296 deposit, south-central Yukon [Ph.D. thesis]: Edmonton, University of Alberta, 307 p., 297 <https://doi.org/10.7939/R3Q23RD6K>.
- Rasmussen, K.L., 2013, The timing, composition, and petrogenesis of syn- to post-accretionary 304 magmatism in the northern Cordilleran miogeocline, eastern Yukon and southwestern 305 Northwest Territories [Ph.D. thesis]: Vancouver, University of British Columbia, 788 p., 306 <https://doi.org/10.14288/1.0071986>.
- Saylor, J.E., and Sundell, K.E., 2016, Quantifying comparison of large detrital geochronology 324 data sets: *Geosphere*, v. 12, p. 203–220, <https://doi.org/10.1130/GES01237.1>.

Vermeesch, P., 2013, Multi-sample comparison of detrital age distributions: 330 *Chemical Geology*, v. 341, p. 140–146, <https://doi.org/10.1016/j.chemgeo.2013.01.010>; 331 corrigenda available at <https://doi.org/10.1016/j.chemgeo.2016.02.005>, 332 <https://doi.org/10.1016/j.chemgeo.2014.07.008>, 333 <https://doi.org/10.1016/j.chemgeo.2013.12.009>.